Liu *et al. Chin. J. Mech. Eng.* (2021) 34:11
https://doi.org/10.1186/s10033-020-00523-6

Chinese Journal of Mechanical Engineering

ORIGINAL ARTICLE

Open Access

Research on Key Issues of Consistency Analysis of Vehicle Steering Characteristics

Yanhua Liu, Xin Guan, Pingping Lu* and Rui Guo

Abstract

Given the global lack of effective analysis methods for the impact of design parameter tolerance on performance deviation in the vehicle proof-of-concept stage, it is difficult to decompose performance tolerance to design parameter tolerance. This study proposes a set of consistency analysis methods for vehicle steering performance. The process of consistency analysis and control of automotive performance in the conceptual design phase is proposed for the first time. A vehicle dynamics model is constructed, and the multi-objective optimization software Isight is used to optimize the steering performance of the car. Sensitivity analysis is used to optimize the design performance value. The tolerance interval of the performance is obtained by comparing the original car performance value with the optimized value. With the help of layer-by-layer decomposition theory and interval mathematics, automotive performance tolerance has been decomposed into design parameter tolerance. Through simulation and real vehicle experiments, the validity of the consistency analysis and control method presented in this paper are verified. The decomposition from parameter tolerance to performance tolerance can be achieved at the conceptual design stage.

Keywords: Interval mathematical theory, Layer by layer decomposition theory, Consistency of performance, Multi-objective optimization

1 Introduction

Performance consistency refers to the dynamic performance consistency of a mass-produced vehicle [1]; this is representative of the quality of the vehicle. It is relatively easy to ensure the performance of a car; however, ensuring that all cars are simultaneously near the ideal target value is difficult, and there are no particularly stringent requirements for part manufacturing, which is a major challenge for automotive design and performance engineers. At present, multi-objective optimization software [2–6], such as Isight, is used in the industry. The performance of the target vehicle is satisfied by optimizing the sensitive parameters. However, ensuring that these target performances can be achieved for all benchmark cars, i.e., designing the part tolerances to ensure that the dynamic performance of the vehicle is within an allowable tolerance range, has not previously been addressed. Even though this has been studied by various scholars, it remains only in a state of research and there is no developed method for reference.

A domestic car is adopted as an example. First, the target steering performance parameters are obtained by testing the performance [7–11]. The performance target parameters are optimized to obtain their performance tolerance interval. Next, the model is established to analyze the sensitivity of the steering, tire, and suspension characteristic parameters and the steering performance of the vehicle [12–14], and to determine the key parameters that affect steering performance. Finally, the performance of the vehicle is verified via a consistency simulation analysis of the target performance interval decomposition method [15–20] and the deviation intervals of the steering, tire, and suspension characteristic parameters are obtained. The results show that the decomposition from vehicle performance tolerance to parameter tolerance can be effectively realized during the conceptual design stage through the consistency analysis and control process established in this study.

*Correspondence: 13604434859@163.com
State Key laboratory of Automobile Simulation and Control, Jilin University, Changchun 200240, China

2 Process of Consistency Research

According to the global investigation and research of relevant theories, there is no complete set of process methods in the literature that are suitable for determining how to decompose the performance tolerance to the consistency design on the hard points, which means the key joint point between body and chassis components, assembly features, and functional components. Therefore, through self-exploration, the three-step process for the vehicle performance consistency analysis and control is presented below:

(1) The target performance is decomposed into the hard points and assembly characteristics;
(2) Related coupling analysis of the sensitivity parameters and performance;
(3) The performance tolerance interval is decomposed into feature tolerance and hard point deviation of the assembly.

3 Interval Decomposition Theory of Objective Performance Tolerance

3.1 Interval Mathematics Theory—Numerical Differentiation Theory

It is very difficult to obtain the derivative of the design parameter reference point analytically because of the complexity of the steering performance dynamics model. Therefore, a numerical method is adopted to realize the derivation of the design parameters at the base point. The principle is to use the discrete method to approximate the value of the derivative based on the value of the function at some discrete points.

The formula for the center difference quotient is expressed as following: If the function $y=f(x)$ is continuous in $[a,b]$ the upper third order, it exists $x-h,x,x+h\in[a,b]$, which makes

$$f'(x)\approx\frac{f(x+h)-f(x-h)}{2h}, \tag{1}$$

and $\xi=\xi(x)\in[a,b]$, obtaining:

$$f'(x)=\frac{f(x+h)-f(x-h)}{2h}+R_c(f,h), \tag{2}$$

where $h(h>0)$ is a small increment of the absolute value. The truncation error of the first derivative approximation of Eq. (2), $f'(x)$, is:

$$R_c(f,h)=-\frac{h^2}{6}f'''(\xi)=O\left(h^2\right). \tag{3}$$

Eq. (1) is referred to as the first derivative central difference formula.

3.2 Taylor Expansion for Asymmetric Structure

First, assume m target performance functions, $f_1(X),f_2(X),f_3(X),\cdots,f_m(X)$, and n independent variables, $X=(x_1,x_2,x_3,\cdots,x_n)$. The m function is ignored for the higher-order terms. At this point $X=(x_1,x_2,x_3,\cdots,x_n)$ can be expanded into the Taylor series:

$$\begin{cases} f_1(X)\approx f_1\left(x_1^c,x_2^c,\ldots,x_n^c\right)+f_{1x_1}\left(x_1^c,x_2^c,\ldots,x_n^c\right)\left(x_1-x_1^c\right)+\ldots \\ \quad +f_{1x_n}\left(x_1^c,x_2^c,\ldots,x_n^c\right)\left(x_n-x_n^c\right), \\ f_2(X)\approx f_2\left(x_1^c,x_2^c,\ldots,x_n^c\right)+f_{2x_1}\left(x_1^c,x_2^c,\ldots,x_n^c\right)\left(x_1-x_1^c\right)+\ldots \\ \quad +f_{2x_n}\left(x_1^c,x_2^c,\ldots,x_n^c\right)\left(x_n-x_n^c\right), \\ \vdots \\ f_m(X)\approx f_m\left(x_1^c,x_2^c,\ldots,x_n^c\right)+f_{mx_1}\left(x_1^c,x_2^c,\ldots,x_n^c\right)\left(x_1-x_1^c\right)+\ldots \\ \quad +f_{mx_n}\left(x_1^c,x_2^c,\ldots,x_n^c\right)\left(x_n-x_n^c\right). \end{cases} \tag{4}$$

$$i=1,2,\cdots,m;j=1,2,\cdots,n,$$

where $f_{ixj}\left(x_1^c,x_2^c,\ldots,x_n^c\right)$ represents the value of the partial derivative at point $\left(x_1^c,x_2^c,x_3^c,\ldots,x_n^c\right)$.

Moving $f_i\left(x_1^c,x_2^c,\ldots,x_n^c\right)$ to the left-hand side of the equation:

$$\begin{cases} f_1(X) - f_1\left(x_1^c, x_2^c, \ldots, x_n^c\right) \approx f_{1x_1}\left(x_1^c, x_2^c, \ldots, x_n^c\right)\left(x_1 - x_1^c\right) + \ldots \\ \quad + f_{1x_n}\left(x_1^c, x_2^c, \ldots, x_n^c\right)\left(x_n - x_n^c\right), \\ f_2(X) - f_2\left(x_1^c, x_2^c, \ldots, x_n^c\right) \approx f_{2x_1}\left(x_1^c, x_2^c, \ldots, x_n^c\right)\left(x_1 - x_1^c\right) + \ldots \\ \quad + f_{2x_n}\left(x_1^c, x_2^c, \ldots, x_n^c\right)\left(x_n - x_n^c\right), \\ \qquad\qquad \vdots \\ f_m(X) - f_m\left(x_1^c, x_2^c, \ldots, x_n^c\right) \approx f_{mx_1}\left(x_1^c, x_2^c, \ldots, x_n^c\right)\left(x_1 - x_1^c\right) + \ldots \\ \quad + f_{mx_n}\left(x_1^c, x_2^c, \ldots, x_n^c\right)\left(x_n - x_n^c\right). \end{cases} \tag{5}$$

This can be rearranged to obtain:

$$\begin{cases} \Delta f_1 \approx f_{1x1}\left(x_1^c, x_2^c, \cdots, x_n^c\right)\Delta x_1 \cdots \\ \quad f_{1xn}\left(x_1^c, x_2^c, \cdots, x_n^c\right)\Delta x_n, \\ \Delta f_2 \approx f_{2x1}\left(x_1^c, x_2^c, \cdots, x_n^c\right)\Delta x_1 \cdots \\ \quad f_{2xn}\left(x_1^c, x_2^c, \cdots, x_n^c\right)\Delta x_n, \\ \qquad \vdots \\ \Delta f_m \approx f_{mx1}\left(x_1^c, x_2^c, \cdots, x_n^c\right)\Delta x_1 \cdots \\ \quad f_{mxn}\left(x_1^c, x_2^c, \cdots, x_n^c\right)\Delta x_n, \end{cases} \tag{6}$$

where $\Delta f_i = f_i(X) - f_i(X^c)$ represents the change in function relative to the deviation point $f_i(X^c)$. $\Delta x_i = x_i - x_i^c$ represents the change in the independent variable, x_i, relative to the deviation point x_i^c, and $f_i xj\left(x_1^c, x_2^c, \cdots, x_n^c\right)$ represents the value of the partial derivative at the point $\left(x_1^c, x_2^c, x_3^c, \cdots, x_n^c\right)$

Finally, we obtain:

$$\begin{cases} \Delta f_1(\Delta X) \approx a_{11}\Delta x_1 + a_{12}\Delta x_2 + \cdots + a_{1n}\Delta x_n, \\ \Delta f_2(\Delta X) \approx a_{21}\Delta x_1 + a_{22}\Delta x_2 + \cdots + a_{2n}\Delta x_n, \\ \qquad \vdots \\ \Delta f_m(\Delta X) \approx a_{m1}\Delta x_1 + a_{m2}\Delta x_2 + \cdots + a_{mn}\Delta x_n, \end{cases} \tag{7}$$

where

$$i = 1, 2, \cdots, m; j = 1, 2, \cdots, n,$$

$$a_{ij} = f_{ix_j}\left(x_1^c, x_2^c, \cdots, x_n^c\right).$$

The equation is deformed and the matrix expression is as follows:

$$\begin{bmatrix} a_{11} & a_{12} & \cdots & a_{1n} \\ a_{21} & a_{22} & \cdots & a_{2n} \\ \vdots & \vdots & \ddots & \vdots \\ a_{m1} & a_{m2} & \cdots & a_{mn} \end{bmatrix} \begin{bmatrix} \Delta x_1 \\ \Delta x_2 \\ \vdots \\ \Delta x_n \end{bmatrix} = \begin{bmatrix} \Delta f_1(\Delta X) \\ \Delta f_2(\Delta X) \\ \vdots \\ \Delta f_m(\Delta X) \end{bmatrix}, \tag{8}$$

namely,

$$\boldsymbol{A}_{m\times n}\boldsymbol{X}_{n\times 1} = \boldsymbol{b}_{m\times 1}, \tag{9}$$

where

$$\boldsymbol{A}_{m\times n} = \begin{bmatrix} a_{11} & a_{12} & \cdots & a_{1n} \\ a_{21} & a_{22} & \cdots & a_{2n} \\ \vdots & \vdots & \ddots & \vdots \\ a_{m1} & a_{m2} & \cdots & a_{mn} \end{bmatrix},$$

$$\boldsymbol{X}_{n\times 1} = \begin{bmatrix} \Delta x_1 \\ \Delta x_2 \\ \vdots \\ \Delta x_n \end{bmatrix}, \boldsymbol{b}_{m\times 1} = \begin{bmatrix} \Delta f_1(\Delta X) \\ \Delta f_2(\Delta X) \\ \vdots \\ \Delta f_m(\Delta X) \end{bmatrix}.$$

The interval mathematical theory is now introduced, assuming the change interval of the independent variable:

$$x_1 = \left[\underline{x}_1, \overline{x}_1\right], x_2 = \left[\underline{x}_2, \overline{x}_2\right], \cdots, x_n = \left[\underline{x}_n, \overline{x}_n\right].$$

The function change interval is:

$$f_1 = \left[\underline{f}_1, \overline{f}_1\right], f_2 = \left[\underline{f}_2, \overline{f}_2\right], \cdots, f_m = \left[\underline{f}_m, \overline{f}_m\right]. \tag{10}$$

By substitution, the system can be expressed as:

$$\begin{cases} \left[\underline{f}_1, \overline{f}_1\right] - f_1\left(x_1^c, x_2^c, \cdots, x_n^c\right) = a_{11}\left(\left[\underline{x}_1, \overline{x}_1\right] - x_1^c\right) + \cdots \\ + a_{1n}\left(\left[\underline{x}_n, \overline{x}_n\right] - x_n^c\right), \\ \left[\underline{f}_2, \overline{f}_2\right] - f_2\left(x_1^c, x_2^c, \cdots, x_n^c\right) = a_{21}\left(\left[\underline{x}_1, \overline{x}_1\right] - x_1^c\right) + \cdots \\ + a_{2n}\left(\left[\underline{x}_n, \overline{x}_n\right] - x_n^c\right), \\ \qquad\qquad \vdots \\ \left[\underline{f}_m, \overline{f}_m\right] - f_m\left(x_1^c, x_2^c, \cdots, x_n^c\right) = a_{m1}\left(\left[\underline{x}_1, \overline{x}_1\right] - x_1^c\right) + \cdots \\ + a_{mn}\left(\left[\underline{x}_n, \overline{x}_n\right] - x_n^c\right). \end{cases} \tag{11}$$

The above equation is obtained using the following:

$$\begin{cases} \left[\Delta\bar{f}_1, \Delta\underline{f}_1\right] = a_{11} \cdot \left[\Delta\underline{x}_1, \Delta\bar{x}_1\right] + a_{12} \cdot \left[\Delta\underline{x}_2, \Delta\bar{x}_2\right] + \cdots + a_{1n} \cdot \left[\Delta\underline{x}_n, \Delta\bar{x}_n\right], \\ \left[\Delta\bar{f}_2, \Delta\underline{f}_2\right] = a_{21} \cdot \left[\Delta\underline{x}_1, \Delta\bar{x}_1\right] + a_{22} \cdot \left[\Delta\underline{x}_2, \Delta\bar{x}_2\right] + \cdots + a_{2n} \cdot \left[\Delta\underline{x}_n, \Delta\bar{x}_n\right], \\ \qquad\qquad\qquad\qquad\qquad\qquad\qquad\qquad\qquad\qquad \vdots \\ \left[\Delta\bar{f}_m, \Delta\underline{f}_m\right] = a_{m1} \cdot \left[\Delta\underline{x}_1, \Delta\bar{x}_1\right] + a_{m2} \cdot \left[\Delta\underline{x}_2, \Delta\bar{x}_2\right] + \cdots + a_{mn} \cdot \left[\Delta\underline{x}_n, \Delta\bar{x}_n\right], \end{cases}$$

where $\left[\Delta\underline{x}_i, \Delta\bar{x}_i\right] = \left[\underline{x}_i - x_i^c, \bar{x}_i - x_i^c\right]$ is the change interval of the independent variable relative to the expansion point and $\left[\Delta\underline{f}_j, \Delta\bar{f}_j\right] = \left[\underline{f}_j - f_j^c, \bar{f}_j - f_j^c\right]$ is the change interval for the function relative to the expansion point.

The matrix expression is obtained by the operation of the interval function:

$$\boldsymbol{A}_{2m\times 2n}\boldsymbol{X}_{2n\times 1} = \boldsymbol{b}_{2m\times 1}, \tag{12}$$

where $\boldsymbol{X}_{2n\times 1} = \begin{bmatrix} \Delta\underline{x}_1 \\ \Delta\bar{x}_1 \\ \Delta\underline{x}_2 \\ \Delta\bar{x}_2 \\ \vdots \\ \Delta\underline{x}_n \\ \Delta\bar{x}_n \end{bmatrix}, \boldsymbol{b}_{2m\times 1} = \begin{bmatrix} \Delta\underline{f}_1 \\ \Delta\bar{f}_1 \\ \Delta\underline{f}_2 \\ \Delta\bar{f}_2 \\ \vdots \\ \Delta\underline{f}_m \\ \Delta\bar{f}_m \end{bmatrix}$.

The upper and lower deviation values of the design parameters $\boldsymbol{A}_{2m\times 2n}$ can be calculated using the $2m\times 2n$ order coefficient matrix. The tolerance of the design parameters is also obtained. This method is referred to as the asymmetric interval Taylor expansion algorithm.

3.3 Algorithm for the Least-Squares Generalized Inverse Interval

3.3.1 Generalized Inverse Matrix

Given the matrix $\boldsymbol{A} \in C^{m\times n}$, if the matrix $\boldsymbol{X} \in C^{n\times m}$ satisfies some or all of the following [21]:

$$\boldsymbol{AXA} = \boldsymbol{A}, \tag{13}$$

$$\boldsymbol{XAX} = \boldsymbol{X}, \tag{14}$$

$$(\boldsymbol{AX})^H = \boldsymbol{AX}, \tag{15}$$

$$(\boldsymbol{XA})^H = \boldsymbol{XA}. \tag{16}$$

Then $\boldsymbol{X}$ is referred to as a generalized inverse matrix.

3.3.2 Generalized Inverse Matrix Theory Used to Solve Linear Equations

For a given inhomogeneous linear system,

$$\boldsymbol{Ax} = \boldsymbol{b}, \tag{17}$$

where $\boldsymbol{A} \in C^{m\times n}$, $\boldsymbol{b} \in C^m$, and $\boldsymbol{x} \in C^n$ are the unknown undetermined vectors. If the existence of vector $\boldsymbol{x}$ sets up the system of linear equations, they are compatible; otherwise, they are referred to as incompatible or inconsistent equations.

The problem of solving linear equations is commonly accompanied by the following situations:

(1) Linear Eq. (17) are compatible with an infinite number of solutions and the general solution of the system of linear equations can be obtained. Simultaneously, if the system of linear equations is compatible, the solution of its extremely small norm can be obtained:

$$\min_{\boldsymbol{Ax}=b} \|\boldsymbol{x}\|, \tag{18}$$

where $\|\cdot\|$ is the Euclidean norm and the solution of the minimal norm that satisfies this condition is unique.

2 If the system of linear Eq. (17) are incompatible, there is no solution in the usual sense. However, in many practical engineering problems, a set of extremum solutions is required.

$$\min_{\boldsymbol{x}\in C^n} \|\boldsymbol{Ax} - \boldsymbol{b}\| \tag{19}$$

where $\|\cdot\|$ is the Euclidean norm, referred to as the least-squares solution of the contradictory linear equations. In general, the least-squares solution of a system of contradictory equations is not unique. However, in the set of the least-squares solutions, the only solution is that with the smallest norm, referred to as the least-squares solution of the minimal norm:

$$\min_{\min\|\boldsymbol{Ax}-\boldsymbol{b}\|} \|\boldsymbol{x}\|. \tag{20}$$

3.3.3 Solution of Compatible Equations

The necessary and sufficient condition for a linear system of Eq. (17) is

$$AA^{(1)}b = b, \tag{21}$$

and its general solution is as follows:

$$x = A^{(1)}b + \left(I_n - A^{(1)}A\right)y. \tag{22}$$

Its minimal norm solution (unique solution) is

$$x = A^{(1,4)}b, \tag{23}$$

among them, $A^{(1,4)} \in A\{1,4\}$, $y \in C^n$.

3.3.4 Solution of Incompatible Linear Equations

If the system of linear Eq. (17) is incompatible, its least-squares solution is

$$x = A^{(1,3)}b. \tag{24}$$

The least-squares (unique) solution is

$$x = A^{+}b, \tag{25}$$

among them,

$$A^{(1,3)} \in A\{1,3\}.$$

3.3.5 Algorithm for the Least-Squares Generalized Inverse Interval

After Eq. (21), with the difference between the upper and lower deviations of the design parameters and the deviation of the target performance tolerance obtained, the least-squares solution is obtained using the generalized inverse matrix theory. Thus, the minimal norm solution and the least-squares solution are obtained.

(1) When $m = n$ and $\det A \neq 0$, linear Eq. (21) exist and are unique:

$$X = A^{-1}b. \tag{26}$$

2 When $m \neq n$, there is no ordinary inverse matrix.

When $m < n$ and $rank(A|b) = rank(A)$, the system is compatible. The minimal norm solution is:

$$X = A_m^{-}b, \tag{27}$$

where A_m^{-} is the minimum norm generalized inverse, satisfying $\min_{Ax=b} \|x\|$.

When $m < n$ and $rank(A|b) \neq rank(A)$, the system is incompatible. The minimal norm solution is:

$$X = A^{+}b, \tag{28}$$

where A^{+} is the positive inverse, satisfying $\min_{\min \|Ax-b\|} \|x\|$.

When $m > n$ and $rank(A|b) = rank(A)$, the system is compatible. The minimal norm solution is:

$$X = A_m^{-}b \tag{29}$$

satisfying $\min_{\min \|Ax-b\|} \|x\|$.

When $m > n$ and $rank(A|b) \neq rank(A)$, the system is in contradiction. The minimal norm solution is:

$$X = A^{+}b \tag{30}$$

satisfying $\min_{\min \|Ax-b\|} \|x\|$.

For a compatible linear system, its minimum norm generalized inverse A_m^{-} is not unique. However, the minimal norm solution $A_m^{-}b$ is unique. The positive inverse matrix A^{+} is one of the most generalized inverse matrices.

Therefore, the solution of the least-squares solution of the linear equations is transformed into the process of the positive inverse matrix A^{+}.

The least-squares solution of Eq. (21) is obtained:

$$X_{2n\times 1} = A^{+}_{2m\times 2n}b_{2m\times 1}. \tag{31}$$

The tolerance interval of the design parameters is obtained as follows:

$$\begin{cases} x_1 = \left[x_1^c + \Delta\underline{x}_1,\ x_1^c + \Delta\overline{x}_1\right], \\ x_2 = \left[x_2^c + \Delta\underline{x}_2,\ x_2^c + \Delta\overline{x}_2\right], \\ \quad\vdots \\ x_n = \left[x_n^c + \Delta\underline{x}_n,\ x_n^c + \Delta\overline{x}_n\right]. \end{cases} \tag{32}$$

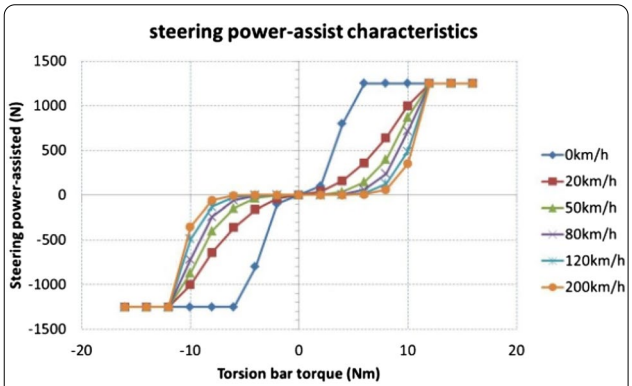

Figure 1 Steering power-assist characteristics

3.4 Operation Steps for the Decomposition of the Performance Tolerance Interval

The decomposition operation steps of the target performance tolerance interval are as follows [22].

3.4.1 Coefficient Gained

Through the method of the center difference quotient, the coefficients of the following Taylor expansion, α_{11}, α_{12},..., α_{mn}, are obtained.

3.4.2 Matrix Established

The coefficient is obtained by combining the center difference quotient method and the asymmetric Taylor expansion method. The mathematical matrix, required for the tolerance calculation, is obtained.

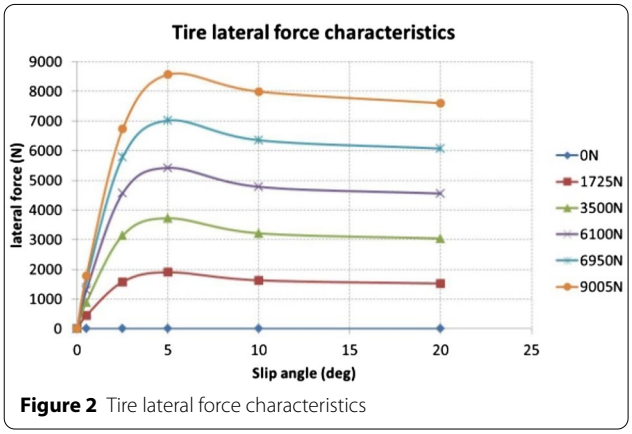

Figure 2 Tire lateral force characteristics

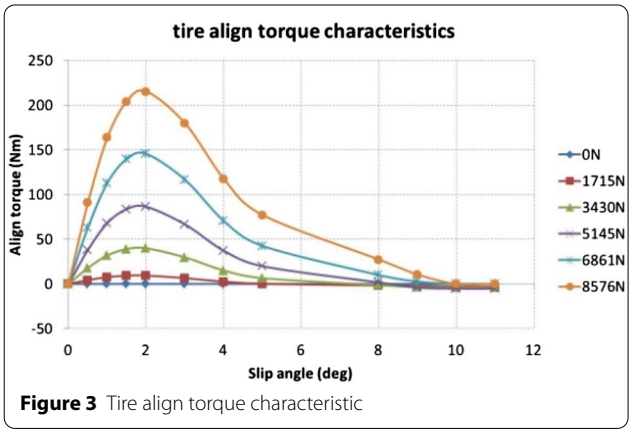

Figure 3 Tire align torque characteristic

3.4.3 Matrix Solved

The mathematical matrix is calculated using the least-squares generalized inverse interval algorithm, obtaining the tolerance interval for the steering system assembly or hard points.

4 Validation of Analysis Method for Steering Characteristic Consistency

4.1 Establishment of the Vehicle Model

The following parameters need to be considered when the vehicle model is built, with the help of the software Carsim.

4.1.1 Steering System

The parameters of the steering system include steering column damping, dry friction, hysteresis; steering gear damping; hysteresis of power steering; and the steering power characteristic. The steering system parameters are shown in Figure 1.

4.1.2 Positioning Parameters of Left and Right Front Wheel Pins

The positioning parameters of the left and right front wheel pins include after the main pin, the main pin inclination, the side distance of the wheel center to the main pin center, and the longitudinal distance of the wheel center to the main pin center.

4.1.3 Wheel Alignment

The wheel alignment includes the initial beam angle of the left and right wheels and their initial external tilt angles.

4.1.4 Tire Characteristics

The tire characteristics include the vertical tire rigidity, lateral force, longitudinal force, positive torque, and tilt-lateral force.

The lateral force characteristics of the tire are shown in Figure 2.

The positive torque characteristics of the tire are shown in Figure 3.

4.1.5 Suspension System

The suspension system includes K left and right suspension characteristics (external dip angle, front beam angle, side angle, lateral displacement of the wheel center, and longitudinal displacement of the wheel center vs. wheel jump) and C left and right suspension characteristics (external dip angle, front beam angle, side angle, lateral displacement of the wheel center, longitudinal displacement of the wheel center vs. longitudinal force, lateral force, and righting torque).

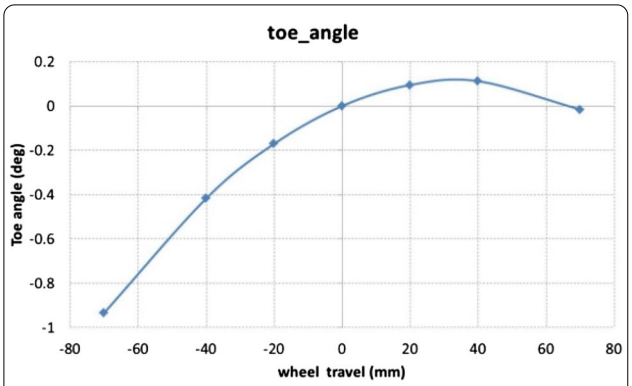

Figure 4 Toe angle change with wheel travel

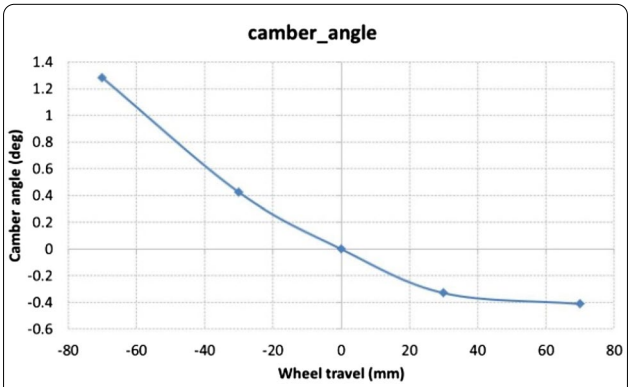

Figure 5 Camber angle change with wheel travel

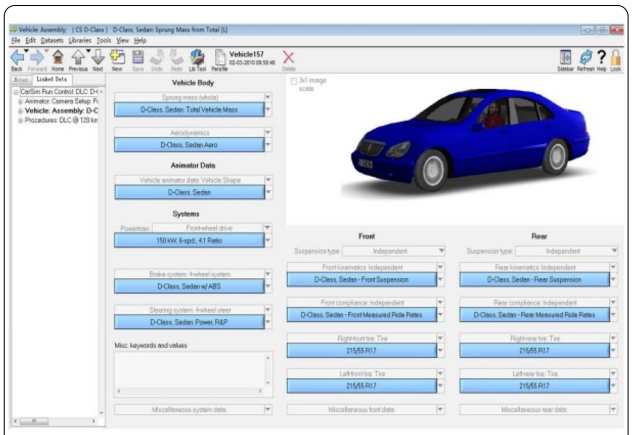

Figure 6 Vehicle model

The main system model parameters of the suspension stiffness and damping are shown in Figures 4, 5.

The vehicle model is established as Figure 6 shown.

4.2 Validation of the Vehicle Model

To verify the accuracy of the dynamic steering performance model in this study, typical experimental steering performance conditions are hereby selected. The accuracy of the model was verified by comparing the experimental data and simulation results. Verification of the specific vehicle steering performance test and simulation comparison is as follows.

4.2.1 Verification of Steady-State Rotation Response

The steady-state circumferential condition is selected to verify the steady-state steering performance of the vehicle. The steady-state steering performance of the model is verified by comparing the experimental and simulation results of the lateral acceleration (Figure 7) and transverse pendulum angular velocity (Figure 8), under steady circumferential motion.

4.2.2 Verification of Transient Steering Response Performance

The transient steering response performance of the vehicle is validated by the experimental conditions of the angular step and angular pulse of the steering wheel. By comparing the real vehicle experimental and simulation values of lateral acceleration and yaw rate under steering wheel angular step and angular pulse motion, the corresponding transient steering performance accuracy of the model is verified.

The lateral acceleration and yaw rate are shown in Figures 9 and 10.

4.2.3 Verification of Steering Portability

The steering portability performance of the vehicle is validated by the experimental conditions of S shape rotation of the steering wheel. By comparing the real vehicle experimental and simulation values of steering torque and yaw rate under steering wheel S shape rotation, the corresponding steering performance accuracy of the model is verified.

The yaw rate and steering torque are shown in Figures 11 and 12.

4.2.4 Verification of Turn-Back Performance

In this study, the experimental conditions of low-speed and high-speed hand-off are selected to verify

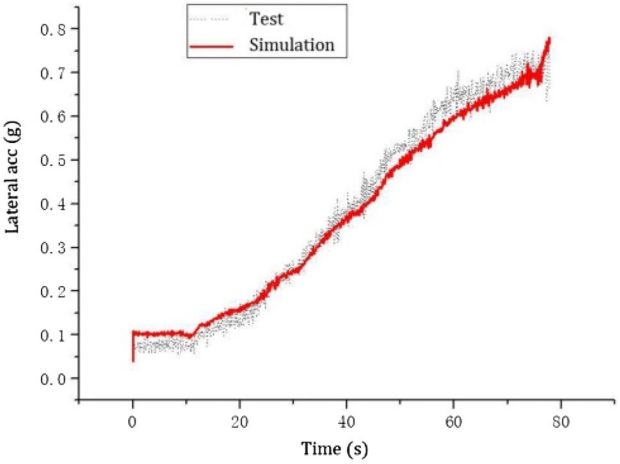

Figure 7 Lateral acceleration

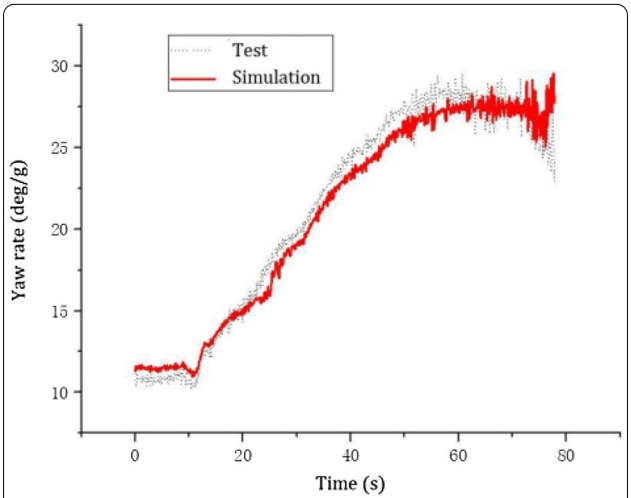

Figure 8 Yaw rate

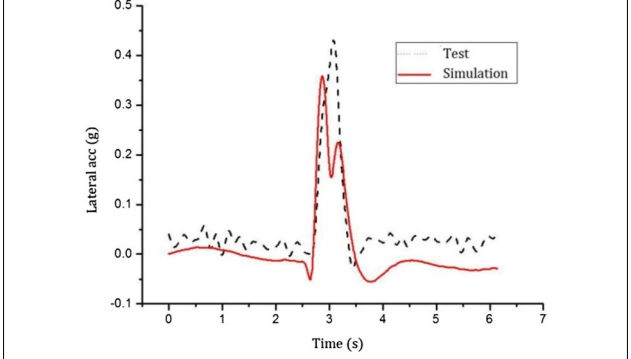

Figure 9 Lateral acceleration

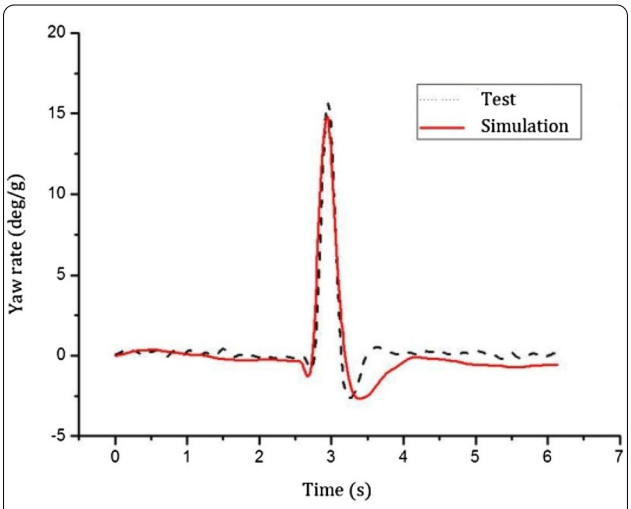

Figure 10 Yaw rate

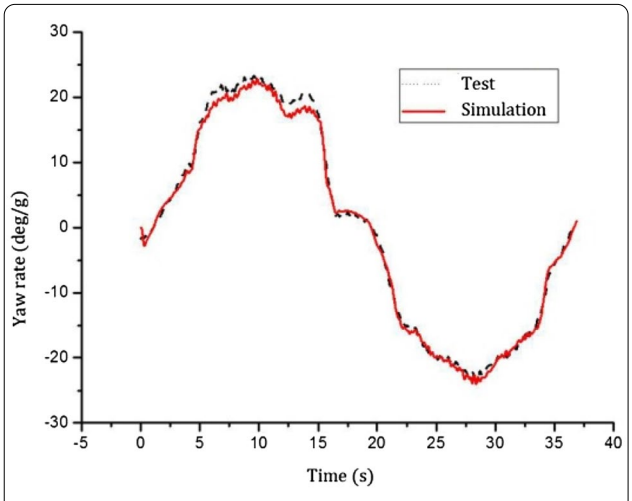

Figure 11 Yaw rate

the steering performance of the vehicle. The simulation results show that the steering performance of the model is correct by comparing the real vehicle experimental and simulation results of the lateral acceleration and yaw rate under the motion of a low-speed and high-speed hand-off. Figures 13 and 14 show the experimental and simulation comparison of a high-speed hand-off vehicle.

4.3 Determination of Steering Target

In this study, the vehicle steering wheel torque and TB factors are selected as the target performance indicators for the consistency analysis of vehicle steering characteristics. The TB factor is obtained by multiplying the peak response time of the yaw rate by the steady lateral

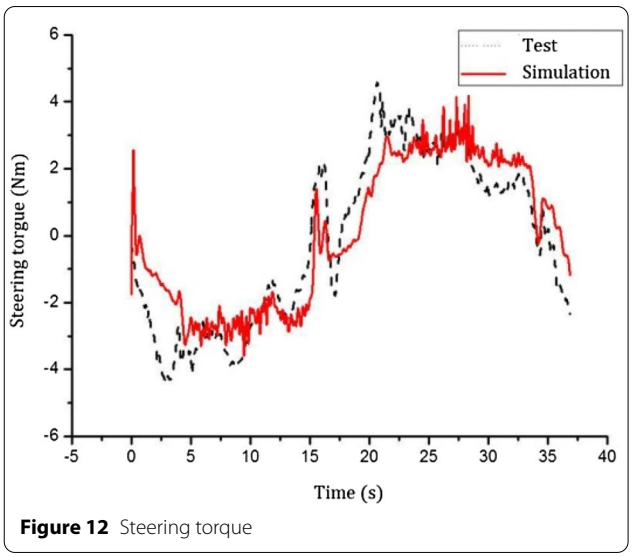

Figure 12 Steering torque

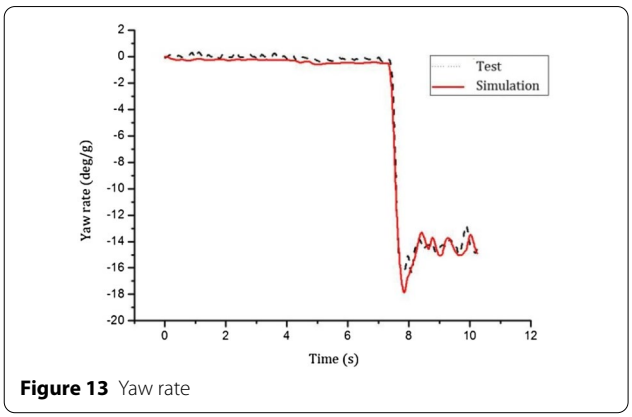

Figure 13 Yaw rate

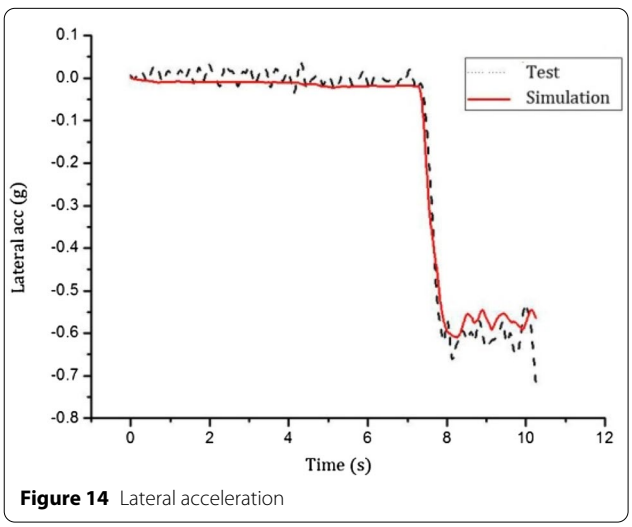

Figure 14 Lateral acceleration

Table 1 Original steering performance value

Index	Initial value
Steering wheel torque	4.5569
TB factor	1.4196

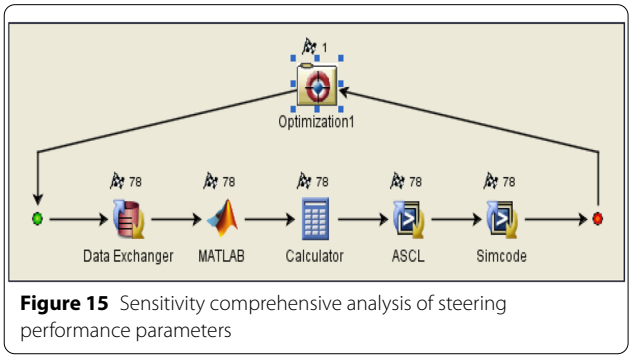

Figure 15 Sensitivity comprehensive analysis of steering performance parameters

deflection angle of the center of mass of the vehicle. The simulation condition is the steering wheel angle step condition in the test of the vehicle steering transient response performance. The speed is 80 km/h and the steering wheel angle corresponds to a lateral acceleration of 0.2*g*.

The original steering performance value is shown in Table 1.

4.4 Comprehensive Analysis of Parameter Sensitivity for Steering Performance According to the Target System

To obtain the sensitivity of the system parameters relative to the steering wheel torque and TB factor [23–25], Carsim software and Isight software were combined for simulation analysis; the results are shown in Figure 15.

4.5 Optimization Design for Steer Target Performance

Optimization of the steering target performance with Isight software and Carsim is presented [26–28] and the theory is utilized for multi-island genetic optimization [29–34].

4.5.1 Optimization Objectives

The optimization objectives are listed in Table 2.

The initial values and ranges of the optimization parameters are shown in Table 3.

4.5.2 Optimization Results

The optimization results are shown in Table 4.

Table 2 Steering performance target value

Index	Target value
Steering wheel torque	4.32
TB factor	1.24

Table 3 Initial parameter values and optimization range

Parameter	Initial value	Optimize range
A_TOE_L	0	(−0.5 ,0.5)
A_TOE_R	0	(−0.5, 0.5)
CS_FY_COEFFICIENT_FL	-4.50×10^{-4}	$(-4.95\times10^{-4}, -4.05\times10^{-4})$
CS_FY_COEFFICIENT_FR	-4.50×10^{-4}	$(-4.95\times10^{-4}, -4.05\times10^{-4})$
CS_FY_COEFFICIENT_RL	-8.31×10^{-4}	$(-9.14\times10^{-5}, -7.479\times10^{-5})$
CS_FY_COEFFICIENT_RR	-8.31×10^{-4}	$(-9.14\times10^{-5}, -7.479\times10^{-5})$
FS_COMP_COEFFICIENT	35	(31.5 , 38.5)
FY_k11	444.357	(400 , 466.5)
FY_k12	894.186	(805 , 984)
HYS_COL	1.5	(1.35 , 1.65)
Mz_k12	17.9612	(16 , 20)
Mz_k13	38.2152	(34 , 42)
K102	40	(32 , 48)
K112	3.11	(2.5 , 3.7)
kToe2	−0.501756	(−0.55 , −0.45)
kToe4	0.425353	(0.38 , 0.47)

Note:

A_TOE_L: left wheel toe angle for front suspension,

A_TOE_R: right wheel toe angle for front suspension,

CS_FY_COEFFICIENT_FL: front left wheel toe angle rate with lateral force case,

CS_FY_COEFFICIENT_FR: front right wheel toe angle rate with lateral force case,

CS_FY_COEFFICIENT_RL: rear left wheel toe angle rate with lateral force case,

CS_FY_COEFFICIENT_RR: rear right wheel toe angle rate with lateral force case,

FS_COMP_COEFFICIENT: rear wheel rate,

FY_k11: tire lateral force with vertical force 1725 N, tire slip angle 0.5,

FY_k12: tire lateral force with vertical force 2500 N, tire slip angle 0.5,

HYS_COL: steering column friction force,

Mz_k12: tire align torque with vertical force 3430 N, tire slip angle 0.5,

Mz_k12: tire align torque with vertical force 5146 N, tire slip angle 0.5,

K102: steering assist torque with steering wheel torque of 4 N·m and vehicle speed of 80 km/h,

K112: steering assist torque with steering wheel torque of 2 N·m and vehicle speed of 80 km/h.

4.6 Decomposition of the Performance Tolerance Interval

Here, the decomposition of the performance tolerance interval calculation is shown [35–39]. Its role is to decompose the steering performance tolerance interval into the system tolerance interval [40, 41].

The performance tolerance interval is obtained by combining the target performance optimization result with the original design value. The steering moment is [0, 0.2369]. The TB factor is [0, 0.1796]. The Jacobian matrix

Table 4 Optimization results

Parameter	Initial value	Optimize result
A_TOE_L	0	0.0396
A_TOE_R	0	−0.2071
CS_FY_COEFFICIENT_FL	-4.50×10^{-4}	-4.77×10^{-4}
CS_FY_COEFFICIENT_FR	-4.50×10^{-4}	-4.50×10^{-4}
CS_FY_COEFFICIENT_RL	-8.31×10^{-5}	-8.55×10^{-5}
CS_FY_COEFFICIENT_RR	-8.31×10^{-5}	-8.25×10^{-5}
FS_COMP_COEFFICIENT	35	32.6579
FY_k11	444.357	482.1273
FY_k12	894.186	855.736
HYS_COL	1.5	1.5797
Mz_k12	17.9612	16.5643
Mz_k13	38.2152	41.196
K102	40	44.528
K112	3.11	3.0892
kToe2	−0.501756	−0.4831
kToe4	0.425353	0.3957

is obtained from the consistency analysis theory, and is shown as follows:

$$
\boldsymbol{A}=\begin{bmatrix}
0.1210 & 0 & 0 & -0.0850 & 0.0460 & 0 & 0.0320 & 0 & 0 & -0.005 \\
0 & 0.1210 & -0.0850 & 0 & 0 & 0.0460 & 0 & 0.0320 & -0.005 & 0 \\
0.0580 & 0 & 0.0030 & 0 & 0.0220 & 0 & 0.0130 & 0 & 0.093 & 0 \\
0 & 0.0580 & 0 & 0.0030 & 0 & 0.0220 & 0 & 0.0130 & 0 & 0.093 \\
0 & -0.0030 & 0.1500 & 0 & 0 & -0.0600 & 0 & -0.0310 & 0.0080 & 0 & 0 \\
-0.0030 & 0 & 0 & 0.1500 & -0.0600 & 0 & -0.0310 & 0 & 0 & 0.0080 & -0.0001 \\
0.0510 & 0 & 0 & 0 & 0.7230 & 0 & 0.4990 & 0 & 0.0930 & 0 & 0 \\
0 & 0.0510 & 0 & 0 & 0 & 0.7230 & 0 & 0.4990 & 0 & 0.0930 & 0 \\
-0.0001 & 0 & -0.0020 & 0 & -0.0100 & 0 & -0.0100 & 0.0325 & 0 & 0.0750 & 0 \\
0 & -0.0020 & 0 & -0.0100 & 0 & -0.0100 & 0 & 0 & 0.0325 & 0 & 0.0750 \\
0 & 0 & 0 & 0.1800 & 0 & 0.1600 & 0 & 0 & -0.0045 & 0.0250 & 0 \\
0 & 0 & 0 & 0 & 0.1800 & 0 & 0.1600 & -0.0045 & 0 & 0 & 0.0250
\end{bmatrix},
$$

$$
\boldsymbol{b}=\begin{bmatrix} 0 \\ 0.2369 \\ 0 \\ 0.1796 \end{bmatrix}.
$$

Solving the following:

$$\boldsymbol{A}_{4\times32}\boldsymbol{X}_{32\times1}=\boldsymbol{b}_{4\times1},$$

we obtain:

$$
\boldsymbol{result}=\begin{bmatrix}
0.0324 & -0.3665 & 0.0123 & 0.0078 & 0.0080 & 0.0033 & 0.0172 & -0.0290 & 0.0250 & 0.0306 \\
0.5325 & -0.0093 & 0.2024 & 0.1404 & 0.0146 & 0.0080 & 0.6484 & 0.1108 & 0.0776 & 0.0497 \\
-0.0002 & -0.0086 & 0.0141 & 0.0078 & 0.0030 & 0.0166 & & & & \\
0 & -0.0002 & 0.0281 & 0.0249 & 0.1391 & 0.3283 & & & &
\end{bmatrix}.
$$

Table 5 Consistency analysis results

Index	Optimize result
Steering wheel torque	(4.32 , 4.5569)
TB factor	(1.24 , 1.4196)
Parameter	**Optimize result**
A_TOE_L	(0.0437, 0.0607)
A_TOE_R	(−0.2830, −0.2090)
CS_FY_COEFFICIENT_FL	$(-5.7338\times10^{-4}, -4.8273\times10^{-4})$
CS_FY_COEFFICIENT_FR	$(-5.1340\times10^{-4}, -4.5370\times10^{-4})$
CS_FY_COEFFICIENT_RL	$(-8.6774\times10^{-5}, -8.6209\times10^{-5})$
CS_FY_COEFFICIENT_RR	$(-8.3140\times10^{-5}, -8.2752\times10^{-5})$
FS_COMP_COEFFICIENT	(33.2196, 55.4817)
FY_k11	(371.7201, 535.547)
FY_k12	(877.1294, 922.1411)
HYS_COL	(1.628, 1.6582)
Mz_k12	(16.561, 16.5643)
Mz_k13	(40.8417, 41.1878)
K102	(45.1559, 45.7792)
K112	(3.1133, 3.1661)
kToe2	(−0.5503, −0.4845)
kToe4	(0.3657, 0.5256)

4.7 Consistency

The consistency analysis results are shown in Table 5.

5 Conclusions

(1) By modeling the steering characteristic parameters and tolerances of the actual system, the feasibility of the methods for expressing the characteristic parameters and tolerance model in the consistency analysis are verified.
(2) According to the vehicle steering performance and characteristic parameters sensitivity analysis, the feasibility of the comprehensive analysis method of correlation and coupling between performance and parameters is verified.
(3) The feasibility of the consistency design process method is verified by decomposing the tolerance interval of the actual steering performance index.

Acknowledgements
The authors would like to express sincere gratitude to the State Key Laboratory of Automobile Simulation and Control for providing the test environment.

Authors' contributions
YL is responsible for writing the entire paper and conducting the simulation model. XG provided advice on the abstract. PL reviewed the introduction and RG checked the validation results. All authors read and approved the final manuscript.

Authors' Information
Yanhua Liu, born in 1973, is currently an engineer at *Brilliance Auto R&D Center, Shenyang, China*. He received his master's degree from *Jilin University, China*, in 2011. His research interests include the chassis system and dynamic simulation. Tel: +86-24-88412628.

Xin Guan, Doctor of Engineering, distinguished Professor of Cheung Kong scholar. He is the president of *Automobile Research Institute of Jilin University, China*. The vice president of *Automobile Engineering Society of China*, and the counselor of Jilin Provincial Government.

Pingping Lu is a teacher at *Jilin University, China*. She received her doctor degree from *Jilin University, China*, in 2012. Her research interests include the chassis system and dynamic simulation.

Rui Guo is a teacher at *Jilin University, China*. She received her doctor degree from *Jilin University, China*, in 2009. Her research interests include the chassis system and dynamic simulation.

Funding
Not applicable.

Competing interests
The authors declare that they have no competing interests.

Received: 27 June 2019 Revised: 12 November 2020 Accepted: 25 November 2020
Published online: 11 January 2021

References

[1] X Guan. *Research progress of vehicle dynamics modeling and simulation in national key laboratory of vehicle dynamics*. Changchun: Academic Report of National Key Laboratory of Automobile Dynamic Simulation of Jilin University, 2009.

[2] L X Zhang, J Q Liu, F Q Pan, et al. Multi-objective optimization study of vehicle suspension based on minimum time handling and stability. *Proceedings of the Institution of Mechanical Engineers*, 2020, 234(9): 2355-2363.

[3] H Xu, Y Q Zhao, C Ye, et al. Integrated optimization for mechanical elastic wheel and suspension based on an improved artificial fish swarm algorithm. *Advances in Engineering Software*, 2019: 137.

[4] Q Shi, C W Peng, Y K Chen, et al. Robust kinematics design of MacPherson suspension based on a double-loop multi-objective particle swarm optimization algorithm. *Journal of Automobile Engineering*, 2019, 233(12): 3263-3278.

[5] X Guan, S Y Feng, J Zhan, et al. Solve the Angle and position of the spindle axis based on steering geometry. *Engineering Science and Technology*, 2009, 9(21): 6593-6596.

[6] J J Hu, Z B He, P Ge, et al. Modeling and simulation of electric power steering system based on multi-body dynamics. *Applied Mechanics and Materials*, 2012, 1498: 2091-2097.

[7] H Spencer, R X Ning. *Virtual product development technology*. Beijing: China Machine Press, 2002.

[8] X M Shi. *Automobile chassis innovation research and development and computer simulation*. Changchun: Academic Report of National Key Laboratory of Automobile Dynamic Simulation of Jilin University, 2006.

[9] T D Kim, J H Kim, J H Kim. Sensitivity analysis and optimum design of energy harvesting suspension system according to vehicle driving conditions. *Journal of the Korean Society for Precision Engineering*, 2019, 36(12): 1173-1181.

[10] E Sert, P Boyraz. Optimization of suspension system and sensitivity analysis for improvement of stability in a midsize heavy vehicle. *Engineering Science and Technology, an International Journal*, 2017, 20(3): 997-1012.

[11] M Sandim, A Paiva, L H D Figueiredo. Simple and reliable boundary detection for mesh free particle methods using interval analysis. *Journal of Computational Physics*, 2020, 420.

[12] Y H Ma, Y F Wang, C Wang, et al. Interval analysis of rotor dynamic response based on Chebyshev polynomials. *Chinese Journal of Aeronautics*, 2020, 9: 2342–2356.

[13] L M Tang, Y Xiao, J W Xie. Fatigue cracking checking of cement stabilized macadam based on measurement uncertainty and interval analysis. *Construction and Building Materials*, 2020, 250.

[14] J W Fan, H H Tao, R Pan, et al. An approach for accuracy enhancement of five-axis machine tools based on quantitative interval sensitivity analysis. *Mechanism and Machine Theory*, 2020, 148: 103806.

[15] H B Huang, J H Wu, X R Huang, et al. A novel interval analysis method to identify and reduce pure electric vehicle structure-borne noise. *Journal of Sound and Vibration*, 2020, 475: 115258.

[16] Z Li, L Zheng. Integrated design of active suspension parameters for solving negative vibration effects of switched reluctance-in-wheel motor electrical vehicles based on multi-objective particle swarm optimization. *Journal of Vibration and Control*, 2019, 25(3): 639-654.

[17] M H Shojaeefard, A Khalkhali, S Yarmohammadisatri. An efficient sensitivity analysis method for modified geometry of Macpherson suspension based on Pearson correlation coefficient. *Vehicle System Dynamics*, 2017, 55(6): 827-852.

[18] H Taghavifar, S Rakheja. Parametric analysis of the potential of energy harvesting from commercial vehicle suspension system. *Journal of Automobile Engineering*, 2019, 233(11): 2687-2700.

[19] R K Ding, R C Wang, X P Meng, et al. Energy consumption sensitivity analysis and energy-reduction control of hybrid electromagnetic active suspension. *Mechanical Systems and Signal Processing*, 2019, 134(Dec.1): 106301.1-106301.20.

[20] Y Q Zhao, H Xu, Y J Deng, et al. Multi-objective optimization for ride comfort of hydro-pneumatic suspension vehicles with mechanical elastic wheel. *Journal of Automobile Engineering*, 2019, 233(11): 2714-2728.

[21] B R Fang, J D Zhou, Y M Li. *Matrix theory*. Beijing: Tsinghua University Press, 2004.

[22] W B Guo, M S Wei. *Singular value decomposition and its application in generalized inverse theory*. Beijing: Science Press, 2008.

[23] X B Ma, P K Wong, J Zhao. Practical multi-objective control for automotive semi-active suspension system with nonlinear hydraulic adjustable damper. *Mechanical Systems and Signal Processing*, 2019, 117: 667-688.

[24] A Khadr, A Houidi, L Romdhane. Design and optimization of a semi-active suspension system for a two-wheeled vehicle using a full multibody model. *Proceedings of the Institution of Mechanical Engineers. Part K, Journal of Multi-body Dynamics*, 2017, 231(k4): 630-646.

[25] A Seifi, R Hassannejad, M A Hamed. Use of nonlinear asymmetrical shock absorbers in multi-objective optimization of the suspension system in a variety of road excitations. *Proceedings of the Institution of Mechanical Engineers. Part K, Journal of Multi-body Dynamics*, 2017, 231(2): 372-387.

[26] R Soon, L N B Gummadi, K Cao. *Robustness considerations in the design of a stabilizer bar system*. SAE Paper, 2005, 01: 1718.

[27] J Zhou. *Reliability and robustness mindset in automotive product development for global markets*. SAE Paper, 2005, 01: 212.

[28] Narasimhan K, Sharma A K. *Multistage process optimization for manufacturing automotive component using finite element method*. SAE Paper, 2005, 26: 332.

[29] D J Ball, M G Zammit, G C Mitchell. *Program optimization by robust design*. SAE Paper, 2005, 01: 3849.

[30] H An, S Chae, H Kim. *Optimum design of exhaust system using the robust design*. SAE Paper, 2006, 01: 0082.

[31] E G Leaphart. *Application of robust engineering methods to improve ECU software testing*. SAE Paper, 2006, 01: 1600.

[32] A Zutshi, B Avutapalli, D Stagner, et al. *Applying six sigma tools to the rear driveline system for improved vehicle level NVH performance*. SAE Paper, 2007, 01: 2286.

[33] S Lee, W Ha, T Yeo. *Robust design for occupant protection system using Taguchi's method*. SAE Paper, 2007, 01: 3724.

[34] Y Q Zhang. The smoothness analysis and parameter selection of virtual prototype based on orthogonal test. *Automotive Technology*, 2005, 10.

[35] M Yao, G L Wang, K K Zhou. Robust optimization design of structural parameters of vehicle drum brake. *Journal of Agricultural Machinery*, 2005, 36(121): 17-20.

[36] M Q Wang. The application of Taguchi method in the optimization of vehicle body frame stiffness. *Automotive Technology*, 1998, 5: 5-7.

[37] C Y Tang. *The optimal design of vehicle dynamic stability characteristics*. Wuhan: Huazhong University of Science and Technology, 2007.

[38] J H Dong. *Multi-objective optimization method and application research based on microgenetic algorithm*. Changsha: Hunan University, 2010.

[39] Fengli Huang, Jianping Lin, Meipeng Zhong, et al. Multi-objective robust design and optimum algorithm in injection molding processing. *Journal of Tongji University*, 2011, 39(2): 287-291+298.

[40] K Guo, L Chen, Y H Wei. *Optimization and its application*. Beijing: Higher Education Press, 2007.

[41] C Fu, Y Liu, Z Xiao. Interval differential evolution with dimension-reduction interval analysis method for uncertain optimization problems. *Applied Mathematical Modelling*, 2018, 69: 441-452.